Meta-GGAs vs. Hybrid Functionals for Point Defects: The Best of Both Worlds Applied to Layered MnO_2, NiO_2 and $KCoO_2$

Raj K. Sah[1], Michael J. Zdilla[1], Eric Borguet[1], and John P. Perdew[2]
[1]*Department of Physics, Temple University, Philadelphia, PA 19122 and*
[2]*Department of Physics and Engineering Physics, Tulane University, New Orleans, LA 70115*

Defects in a material can significantly tune its properties and enhance its utility. Hybrid functionals like HSE06 are often used to describe solids with defects. However, geometry optimization using hybrid functionals (e.g., HSE06), often used to describe solids with defects, is challenging for a large supercell, as needed for defect study. The proposed r^{2}SCAN+rVV10+U+U_d method, which is computationally much cheaper and faster than hybrid functionals, can successfully describe defects in materials with the proper choice of U (for the d orbitals of the host atom) and U_d (for those of the defect atom), as shown here for small polarons in layered transition-metal oxides. We use a literature value of U or U_d appropriate to a given transition-metal ion and its oxidation state. The materials MnO_2 and NiO_2, with one K atom intercalated between layers in a supercell, are found to have one localized occupied e_g state on the transition metal ion that takes an electron from the K atom, when the geometry is calculated as above, for standard U values but not for $U=U_d=0$. K-intercalated $KCoO_2$ is surprisingly different, due to a dramatic change of electronic configuration of the defected Co^{+2} ion.

I. INTRODUCTION

This work is part of a larger project to predict computationally which layered materials with which patterns of alkali-atom intercalation are promising candidates for catalysis of the oxygen evolution reaction in water splitting for clean hydrogen fuel. Earlier work[1,2] showed the importance of small-polaron defects formed by transfer of an electron from an alkali atom to a neighboring transition-metal ion. Calculation of the polaron requires a nonlocal density functional for the exchange-correlation energy, and geometry optimization in a large supercell. We found that hybrid functionals as used in Ref.[1] are too expensive for a broad materials search. In this article, we show that an alternative r^{2}SCAN+rVV10+U+U_d approach can achieve comparable accuracy at much lower cost. This approach may be useful for other point defects in other materials. We also found that, while one intercalated K atom creates one localized electron in the energy gap of layered MnO_2 and NiO_2, it can create four in layered $KCoO_2$. We further found that, while r^{2}SCAN needs a +U correction to create a polaron in MnO_2 and NiO_2, it does not need one in $KCoO_2$. Our broader computational and experimental materials search is now underway.

Various types of defects exist in solids, and defects in solids can influence numerous important properties like electrical conductivity, reactivity, and magnetic or optical properties. For example, defects like polarons in transition metal oxides (TMOs) favor the Oxygen Evolution Reaction (OER)[1,2]. Leveraging defects as a tool allows fine tuning of the electronic properties of materials, making the understanding of defects in materials a pivotal area of research.

The computational design and study of such materials using first-principles density functional theory (DFT)[3,4] offer valuable early insights. However, studying defects using first-principle DFT presents challenges, as density functional approximations (DFAs) introduce self-interaction error (SIE). Popular DFAs such as LDA/GGA/meta-

GGA tend to underestimate the Perdew-Parr-Levy-Balduz (PPLB)[5] straight line condition, leading to inaccuracies in describing charge transfer that are reduced but not eliminated in that sequence of functionals. Given that defect studies require proper charge transfer, DFAs often fall short in accurately portraying defects in a system.

However, hybrid functionals, which combine a fraction of exact exchange, such as HSE06 which utilizes 25% exact exchange and 75% PBE exchange in the short range along with full PBE exchange in the long range, experience less SIE and provide a more accurate description of the electronic structure of materials. Hybrid functionals have been successfully employed in studying defects in solids. For instance, Peng et al.[1] effectively investigated polaron-like defects in birnessite. Nevertheless, the inclusion of exact exchange in hybrid functionals renders them computationally expensive. The structural relaxation using hybrid functionals becomes particularly costly for a reasonably sized supercell with localized defects, with computational expenses rapidly escalating as the supercell size increases to better simulate defects. Consequently, the structural optimization of large supercells becomes exceedingly challenging, and at times almost impossible. Another challenge associated with hybrid functionals is that the universal exact-exchange mixing parameter is not determined through any exact condition, nor is the range-separation parameter in range-separated hybrids[6]. Peng et al. determined a mixing parameter of 0.22 to study defects in birnessite using HSE06[1], deviating from the original value of 0.25. Additionally, determining a mixing parameter for semiconductors that may not be suitable to metals or insulators[7] adds to the challenge of finding an appropriate parameter for the system under study when employing hybrid functionals.

r^{2}SCAN[8] is a recently developed meta-generalized gradient approximation that reinstates exact constraint adherence to rSCAN[9], preserving the numerical efficiency of rSCAN while simultaneously restoring the transferable accuracy of SCAN[10]. Several studies have demonstrated that SCAN predicts geometries and other properties as well as or even better than hybrid functionals. Sun et al.[6] showed that SCAN accurately predicts geometries and energies of diversely bonded materials and molecules, matching or surpassing the accuracy of computationally expensive hybrid functionals. Another study by Saẏnick and Cocchi on cesium-based photocathode materials Cs_3Sb and Cs_2Te reported excellent performance of SCAN and HSE06 for both structural and electronic properties[11]. A recent paper on the arXiv[12] reports that, while SCAN may not reliably describe the properties of deep defects and small polarons in several semiconductors and insulators, it yields remarkably good agreement with experimental structural parameters for materials like ZnO, GaN, Ga_2O_3 and NaF. Additionally, a study by Varadwaj and Miyake on the geometrical, electronic, and optical properties of vanadium dioxide found that SCAN and SCAN-rVV10 can adequately predict the most important geometrical and optoelectronic properties of VO_2[13]. Numerous related studies further support the idea that SCAN successfully describes the structure and other properties of materials. Given that r^{2}SCAN closely agrees with SCAN in accuracy, we assume that r^{2}SCAN would exhibit similar accuracy in the aforementioned studies.

By construction, r^{2}SCAN can exhibit very small or negligible SIE (as reflected by its smaller Hubbard U correction) and performs at the level of hybrid functionals but demands less computational resource and time. In this study, we demonstrate that the r^{2}SCAN + rVV10 + U + U_d functional can effectively describe the defects in materials at the level of the hybrid functional HSE06, or possibly even better. Here, U represents the Hubbard U correction of Anisimov and collaborators[14–16], applied to transition metal sites other than the defect site, while U_d is the correction applied to the defect site. Cococcioni and de Gironcoli[17] showed that the +U correction can be re-

garded as a many-electron self-interaction correction that, like the PPLB condition[5], penalizes non-integer electron number on a localized orbital to which it is applied.

Additionally, vdW denotes the long-range van der Waal's correction. In our approach, we utilize rVV10[18,19] to account for this interaction, which importantly reduces inter-layer spacing. In many of our calculations, including HSE06 without vdW, we use the supercell volume and shape from $r^2SCAN + rVV10 + U + U_d$, although we can as a check relax the internal coordinates with HSE06.

Transition metal ions, which serve as a site for defect formation in solids, are in different oxidation states (OS) than otherwise-identical ions. For example, in a K-intercalated MnO_2, the polaronic Mn site is in the +3 OS and the remaining Mn ions are in the +4 oxidation state[1,2]. Ions in different OS have different numbers of d electrons. Reference[20] reports that the ideal U correction decreases with increasing OS, which is attributed to a lower number of exchange interactions among fewer d electrons in a higher oxidation state. This behavior has been observed and reported for vanadium ions[20].

However, this situation is not universal, as we can see that U values for Mn for r^2SCAN are 1.5 eV, 2.1 eV and 1.8 eV for Mn ions with average oxidation states +3.5, +2.5 and +2.33 respectively[21]. Here we see that Mn in the +2.5 average OS needs more U correction than Mn in the +2.33 average OS, which does not follow the trend observed for vanadium, but at least U for Mn in the +3.5 average OS supports the trend. However it's obvious for the Mn oxide system that Mn ions in different oxidation states need different U corrections. It is also important to note that U = 1.8 eV, determined for Co ions for SCAN using the oxidation reaction $CoO \rightarrow Co_3O_4$ where Co ions are in +2 and +2.67 oxidation states, wrongly predicted CoO_2 to be non-metallic[20]. However SCAN without U correction correctly predicted CoO_2 (+4 oxidation state) to be metallic[20]. Thus the U value can vary with the oxidation state of ions in the system. This indicates that if a system has transition metal ions in different OS, the proper way to describe such a system would be by applying different U corrections to the transition metal ions based on their OS. This could be because DFAs make different SIE for ions in different OS.

Here we present a successful study of defects in solids by the double U correction $r^2SCAN + rVV10 + U + U_d$ method, where U_d is the U correction applied to the defect site and U is the U correction applied to remaining sites as required for the system. Since U generally increases with decreasing OS, and defect sites are typically in a lower oxidation state, we expect $U_d \geq U$, although exceptions are possible.

One can use the $r^2SCAN + rVV10 + U + U_d$ geometry and the HSE06 hybrid functional orbital energies to leverage the best features of the hybrid functional. It appears that employing the full $r^2SCAN + rVV10 + U + U_d$ and/or HSE06 using $r^2SCAN + rVV10 + U + U_d$ geometry is a state-of-the-art method for studying defects in solids.

II. RESULTS AND DISCUSSION

We choose three layered TMOs, MnO_2, NiO_2, and $KCoO_2$ for our study. Transition metal and oxygen ions in these TMOs are arranged in MO6 (where M=Ni, Mn, Co) octahedron patterns. Inserting an alkali metal ion between the layers creates a polaronic defect, specifically a Jahn-Teller electron small polaron [1]. This defect has been studied in birnessite (MnO_2) using the HSE06 functional [1][22].

A. Layered MnO_2

First, we calculated the one-electron density of states (DOS) for both the pristine and a K-intercalated birnessite using the HSE06 functional with an exact exchange mixing parameter (α) of 0.22 to reproduce the work

of Peng et al.[1]. Comparing Figures 1A and 1B in the current work with Figures 2B and 2C of Peng et al[1], we conclude that we have successfully reproduced the latter's figures 2B and 2C. We found the band gap of pristine birnessite to be 3.4 eV. We observed similar effects upon intercalation of a potassium (K) ion, as observed by Peng et al.[1]. In Figure 1B, a K-intercalated birnessite exhibits the shifting of Mn(III) d-states to higher energy, a polaronic peak at the conduction band (CB) edge, and a break in spin symmetry of the total DOS in the CB. These effects were previously seen and explained by Peng et al.[1]. The shifting of Mn(III) d-states is attributed to increased coulomb repulsion in d orbitals of Mn(III). The spin symmetry of the total DOS in pristine MnO_2 arises from the antiferromagnetic order of the M(IV) ions, and is disrupted by the defect Mn(III) ion (while the other pristine materials are non-magnetic). The appearance of the polaron peak is attributed to e1g states in Mn(III)[1,2].

We will see similar effects upon a K-intercalation in NiO_2 and $KCoO_2$ systems later, and these effects can be understood through similar reasoning. The d-state electronic configurations of Mn(IV) in pristine MnO_2 and Mn(III) in a single K-intercalated MnO_2 are as shown in Fig. 4 A and B respectively.

Swathilakshmi et al.[21] recently determined the optimal U value for r^2SCAN for Mn to be 1.8 eV. They utilized three oxidation reactions: $MnO \rightarrow Mn_2O_3$,$MnO \rightarrow Mn_3O_4$, and $Mn_2O_3 \rightarrow MnO_2$. The U values for these reactions are 2.1 eV, 1.8 eV and 1.5 eV respectively[21]. The average OS of Mn ions in these reactions are +2.5, +2.3 ,and +3.5 respectively[21]. U values for these reactions are small compared to those for the PBE GGA and do not differ significantly, suggesting that r^2SCAN makes a small, comparable SIE but not an equal one for Mn(II), Mn(III) and Mn(IV) ions in manganese oxide systems. The reported optimal U value of 1.8 eV for the Mn ion is the average of U values for the above three oxidation reactions[21].

First, we performed $r^2SCAN + rVV10 + U$ calculations for pristine birnessite with the optimal U of 1.8 eV and obtained the DOS as shown in Figure 2A. $r^2SCAN + rVV10 + U$ predicts a band gap of 2.30 eV for the pristine structure. The underestimation of the band gap compared to HSE06 by meta-GGA/GGA is a general trend. Next, we performed $r^2SCAN + rVV10 + U + U_d$ calculations for a K-intercalated MnO_2. As r^2SCAN exhibits a small SIE, we initially set $U=U_d=0.0$ eV to see the performance of r^2SCAN+rVV10 without U correction. However, this method failed to resolve the defect, as depicted in Figure 2B, suggesting the necessity of a U correction. The corresponding polaron is delocalized, which can be seen by the extra electrons between the CB minimum and the chemical potential or Fermi level at 0 eV. This can be clearly seen in the inset figure. For the description of a polaron in a single K-intercalated MnO_2, DFA has to transfer charge from the inserted K atom to a Mn atom. The charge delocalization error of DFAs prohibits transferring a complete electron from the K atom to the Mn site. This indicates the need for +U correction, which can lower the energy of the defected system by removing the partial occupancy and localizing the electron on the defect site. Subsequently, we tested the optimal U by setting $U=U_d=1.8$ eV and the obtained DOS is shown in Figure 2C, revealing the appearance of a polaronic peak. The +U correction helps to remove the partial occupancy by applying an extra penalty to the partially occupied orbital and lowering its energy. As a result, the polaron is localized and appeared at the CB edge. We see shifting of Mn(III) d-states to higher energy, and spin symmetry breaking in the total DOS in the CB, consistent with the HSE06 results. As discussed in the work by Peng et al.[1] and Ding et al.[2], polaron formation can with the right distribution of intercalated potassium atoms create a potential step between layers. Consequently, the layer without a defect places the conduction band closer in energy

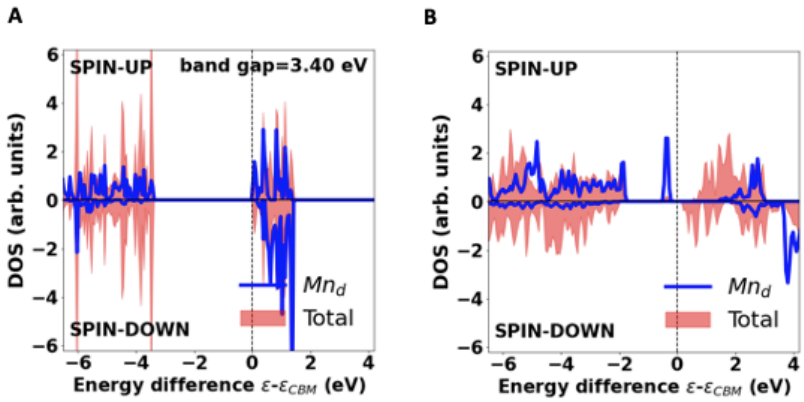

FIG. 1. HSE06 (α = 0.22) spin-resolved density of states per atom in (A) pristine MnO_2 with Mn(IV) ions and (B) MnO_2 with a single intercalated K^+ ion and a defect Mn(III) cation in a supercell with 97 atoms. For comparison with Ref.[1], the interlayer spacing is set to 7.12 Å, and internal coordinates are relaxed in HSE06. In Figs. 1-9 (expect in Figs. 4, and 7), the shaded area shows the total density of one-electron states, and the blue curve shows the transition-metal-d states projected onto the site where the small polaron forms or is expected to form. Also in Figs. 1-9 (expect in Figs. 4, and 7), the peaks (if any) in the band gap below the conduction band minimum (CBM) are occupied, localized states of the defect ion. The energy zero is set to the energy of the lowest-energy unoccupied orbital. The total density has been scaled down to make it comparable in size to the projected Mn-d density of states.

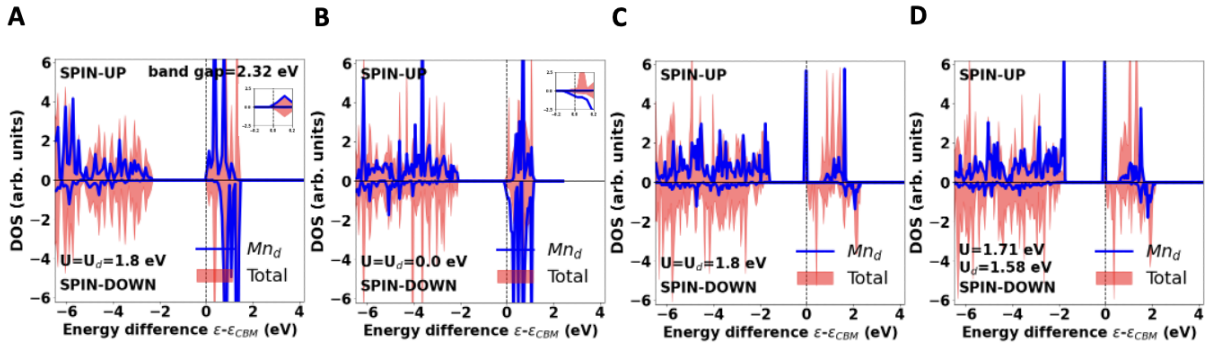

FIG. 2. r^{2}SCAN+rVV10+U+U$_d$ spin-resolved density of states per atom in (A) pristine MnO_2 with U=U$_d$=1.8 eV and in a single K-intercalated MnO_2 with (B) U = U$_d$ = 0.0 eV, (C) U= U$_d$ =1.8 eV, (D) U=1.71 eV and U$_d$ =1.58 eV. The geometry has been optimized in r^{2}SCAN+rVV10+U+U$_d$, which makes the interlayer spacing 5.26 Å. The insets in figures A and B show DOS near the 0 eV region. The inset in figure B shows that for U=U$_d$=0 the extra electron from the intercalated K goes to the bottom of the conduction band, making a semi-metal.

to the polaronic electronic state of the layer with defects. This effect can facilitate the electron transfer process between sheets and any interlayer species and enhance catalytic activity of the material.

Motivated by studies indicating that U depends on OS, and that generally U decreases with an increase in OS, we determined U for the r^{2}SCAN+rVV10+U functional for Mn^{+3} and Mn^{+4} by comparing r^{2}SCAN+rVV10+U's magnetic moment with the HSE06+D3 magnetic moment. For

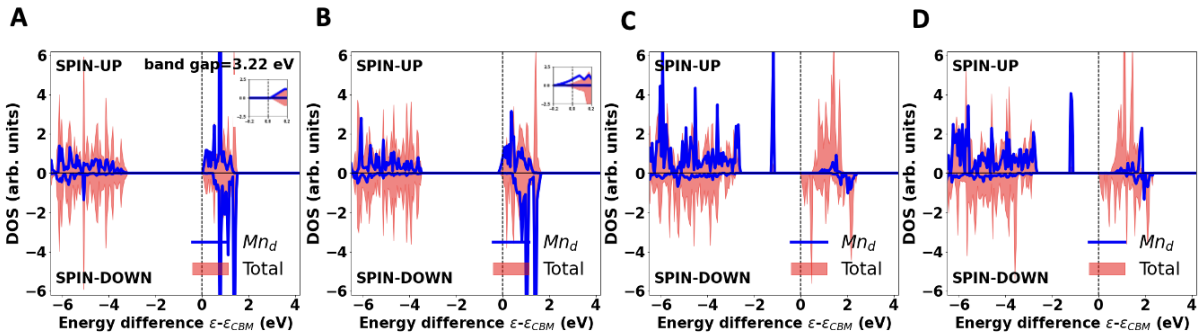

FIG. 3. HSE06+D3 spin-resolved density of states per atom using r^{2}SCAN+rVV10+U+U$_d$ geometry of Fig. 2 in (A) pristine MnO^2 with U=U$_d$=1.8 eV and in a single K-intercalated MnO_2 with (B) U=U$_d$=0.0 eV, (C) U=U$_d$=2.1 eV, (D) U=1.71 eV and U$_d$=1.58 eV. The insets in figures A and B show DOS near the 0 eV region. The inset in figure B shows that for U=U$_d$=0 the extra electron from the intercalated K goes to the bottom of the conduction band, making a semi-metal.

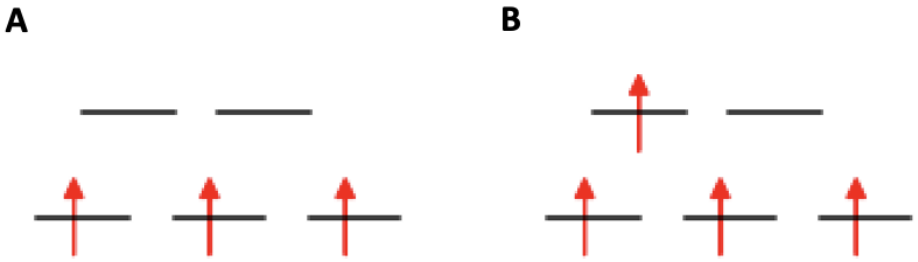

FIG. 4. d-orbital splitting (A) in Mn^{+4} in pristine MnO_2 demonstrating filled t_{2g} states and empty e_g states and (B) in Mn^{+3} in a single K-intercalated MnO_2.

this we used pristine $KMnO_2$ and MnO_2 systems. First, we relaxed the structure using HSE06+D3 and used the structure to get the magnetic moment due to spin charge density within the Wigner-Seitz sphere around an Mn ion. We used the HSE06+D3 geometry for r^{2}SCAN+rVV10+U and slowly increased U in small steps until we got the same magnetic moment as HSE06+D3. This method gave U values of 1.71 eV and 1.58 eV for Mn^{+3} and Mn^{+4} ions respectively. These values are close to the values in reference[21].

We then obtained the r^{2}SCAN+rVV10+U+U$_d$ DOS of a K intercalated MnO_2 with U=1.71 eV and U$_d$=1.58 eV which is as shown in figure 2C. U=1.71 eV and U$_d$=1.58 eV gave similar result to U=U$_d$=1.8 eV.

We also performed HSE06+D3 calculations on the r^{2}SCAN+rVV10+U+U$_d$ geometries, and the resulting DOS are plotted in Figure 3. The D3 dispersion correction was used for the HSE06 functional with new D3 damping parameters a1 = 0.383, a2 = 5.685, and s8 = 2.310 generated for HSE06 functional[23]. For HSE06+D3 calculations, we used an exact exchange mixing parameter (α) of 0.25. This is because we found that the r^{2}SCAN+rVV10+U geometry in much better agreement with the HSE06+D3 geometry for α=0.25 than for 0.22. More details are in the supplementary information.

Fig. 3A shows the HSE06+D3 DOS of pristine MnO_2 obtained using the

r^{2}SCAN+rVV10+U+U$_d$ (U=U$_d$=1.8 eV) geometry. HSE06+D3 increases the band gap of pristine MnO_2, close to the HSE06 result (Figure 1A). Fig. 3B shows the HSE06+D3 DOS of a K-intercalated MnO_2 obtained using the r^{2}SCAN+rVV10+U+U$_d$ (U=U$_d$=0.0 eV) geometry. Like the r^{2}SCAN+rVV10+U+U$_d$ (U=U$_d$=0.0 eV) method, HSE06+D3 also fails to localize the defect state. Fig. 3C shows the HSE06+D3 DOS of a K-intercalated MnO_2 obtained using the r^{2}SCAN+rVV10+U+U$_d$ (U=U$_d$=1.8 eV) geometry. Here, the defect state appears as in the r^{2}SCAN+rVV10+U+U$_d$ (U=U$_d$=1.8 eV) method, but deep in the band gap. Fig. 3D shows the HSE06+D3 DOS of a K-intercalated MnO_2 obtained using the r^{2}SCAN+rVV10+U+U$_d$ (U=1.71 eV and U$_d$= 1.58eV) geometry. Here, also, the defect state appears as in the r^{2}SCAN+rVV10+U+U$_d$ (U=U$_d$=1.8 eV) method, but deep in the band gap.

We also calculated HSE06 and HSE06+D3 DOS using an exact exchange mixing parameter α of 0.22 as determined by Peng et al.[1] on r^{2}SCAN+rVV10+U+U$_d$ geometry with U=U$_d$=1.8 eV and obtained DOS as shown in Fig. S A and B, respectively. As expected, HSE06(α=0.22) and HSE06(α=0.22)+D3 DOS do not look different. Noticeably, HSE06(α=0.22) DOS does not look different from the full HSE06(α=0.25)+D3 evaluated on the same geometry, which is shown in Fig. 3C.

R. Ding et al.[2] have proposed a position of the polaron close to the CB in layered MnO_2 with an alternation of polaron-containing and polaronless layers. This scenario matches better with r^{2}SCAN+rVV10+U+U^d DOS, where the polaron is close to the CB.

r^{2}SCAN+rVV10+U+U$_d$ with U=U$_d$=1.8 eV, and U=1.71 eV and U$_d$=1.58 eV give similar DOS. HSE06+D3 DOS are also similar for those geometries, with the polaron appearing deep in the gap. We found slightly better agreement between the magnetic moment of the defected Mn^{+3} ion between r^{2}SCAN+rVV10+U+U$_d$ and HSE06+D3 for U=1.71 eV and U$_d$=1.53 eV.

We do not have direct experimental DOS results to make a comparison. Thus, it is challenging to conclude which method provides a better description of the defect. However, we can assert that all three methods- HSE06, r^{2}SCAN+rVV10+U+U$_d$ and HSE06+D3 using r^{2}SCAN+rVV10+U+U$_d$ geometry- have successfully described the polaronic defect in birnessite with the proper U and U$_d$ for r^{2}SCAN+rVV10+U+U$_d$ calculations.

B. Layered NiO_2

Our next system under study was a layered NiO_2. This material has a hexagonal crystal structure with space group $P6_3/mmc$. The material project website (https://nextgen.materialsproject.org/) reports that the material is synthesizable but not stable. Whether stable or not, this material is stable enough for our study. Layered NiO_2 has a similar structure to birnessite, where Ni ions are in a +4 OS with completely occupied t_{2g} states[24].

We began the DOS calculation using the r^{2}SCAN+rVV10+U+U$_d$ functional for both pristine and K-intercalated NiO_2 systems. The r^{2}SCAN U value for Ni ions was recently determined by Swathilakshmi et al.[21]. They utilized the oxidation reaction $2Li_2O+4NiO+O_2 \rightarrow 4LiNiO_2$ and obtained a U value of 2.1 eV. In this reaction, the Ni ions exhibit OS of +2 and +3, with an average OS for Ni ions in the reaction calculated to be +2.5.

For the pristine NiO_2, r^{2}SCAN+rVV10+U+U$_d$ with U=U$_d$=2.1 eV, correctly predicted a non-magnetic ground state with a band gap of 1.62 eV, as shown in Fig. 5A. The d-states of Ni(IV) in pristine NiO_2 are split into t_{2g} and e_g states, with t_{2g} states completely occupied and e_g states empty, as shown in Fig. 7A. This gives zero spin to Ni ions and makes the solution non-magnetic. As in the birnessite case, we expect that adding an extra K atom between layers would transfer an electron from the inserted K atom to a Ni site, forming a

defect. The defected Ni site would undergo Jahn-Teller distortion, localizing the electron in the e_g state, as shown in Fig. 7B.

For a K-intercalated NiO_2, we initially used $U=U_d=0.0$ eV to observe how r^{2}SCAN+rVV10 without U correction performs for this system, as r^{2}SCAN makes small SIE, and we obtained the DOS as plotted in Fig. 5B. However, this choice of U and U_d failed to describe the defect state. The polaron is delocalized, which can be seen from the insets to Figs. 5B: The extra electron goes to localized states at the bottom of the conduction band, with fractional occupation on each Ni ion in the supercell. For the description of a polaron in a single K-intercalated NiO_2, DFA has to transfer charge from the inserted K atom to a Ni atom. The charge delocalization error of DFAs prohibits the transfer of complete electrons from the K atom to the Ni site. This indicates the need for +U correction, which can lower the energy of the polaron by removing the partial occupancy and localizing it. We then used the available U value by setting $U=U_d=2.1$ eV and obtained the DOS, as plotted in Fig. 5C. This choice of U values forms a defect at one of the Ni sites. The +U correction helps to remove the partial occupancy by applying an extra penalty to the orbital and lowers the energy of the orbital. As a result, the polaron is localized and appears in the gap just below the CB minimum. The formation of the polaron at the VB edge indicates that a K -intercalated NiO_2 could show catalytic activity similar to that of birnessite by lowering the overpotential. Most of the charge from K atom is transferred to this defect site, which has magnetic moment of 0.786 μ_B . However, we observe a Ni site in another layer picking up small but nonzero magnetic moment of 0.137 μ_B with magnetic moment of all remaining Ni sites smaller than 0.03 μ_B. This suggests that we might need different values of U and U_d for r^{2}SCAN+rVV10+U+U_d to accurately describe charge transfer to the defect site in a K-intercalated NiO_2 system.

The determination of U=2.1 eV for Ni for r^{2}SCAN involves Ni in +2 and +3 states[21], with an average OS of +2.5. Since the precise U values for Ni(III) and Ni(IV) states are not available, we set $U_d=2.1$ eV for NI(III) as the Ni (III) OS is close to +2.5 and searched for different U values for Ni(IV). We observed that increasing U values beyond 2.3 eV transfers more and more charge to a Ni site in another layer than a defect site. So, we lowered the U values (U=1.0 eV and 0.0 eV) and found that lowering the U values slightly improves the solution by lowering the magnetic moment of a Ni site in another layer to 0.06 μ_B without significant change in magnetic moment of the defect site. The DOS plots for U=0.0 eV and $U_d=2.1$ eV doesn't look different from Fig. 5C. We also increased U_d values, keeping U fixed at 2.1 eV, and observed an increase in the magnetic moment of the defect site, reaching 1 μ_B for U=3.8 eV. These are magnetic moments due to the spin charge density inside the Weigner-Seitz sphere. It is important to note that the magnetic moment of the defect site 1.0 doesn't guarantee the full transfer of an electron from the intercalated K atom to the defect site, as this is a magnetic moment inside the Weigner-Seitz sphere, which doesn't reflect the actual magnetic moment of the defect site. However, this analysis shows that one can adjust the U and U_d value for more charge transfer to the defect site where necessary.

We also determined the U value of 2.06 eV for the Ni^{+3} ion by comparing the HSE06+D3 magnetic moment of the ion with the r^{2}SCAN+rVV10+U magnetic moment as discussed in the supplementary material. The magnetic moment here is due to the spin charge density inside the Weigner-Seitz sphere. We couldn't apply this method to get the U value for the Ni^{+4} ion as the magnetic moment of Ni^{+4} ions are zero and the magnetic moment of Ni^{+4} ion in the r^{2}SCAN+rVV10+U calculation of the NiO_2 system remained zero until the U value was significantly large. As this value is not very different from 2.1 eV, we got a similar r^{2}SCAN+rVV10+U+U_d result with

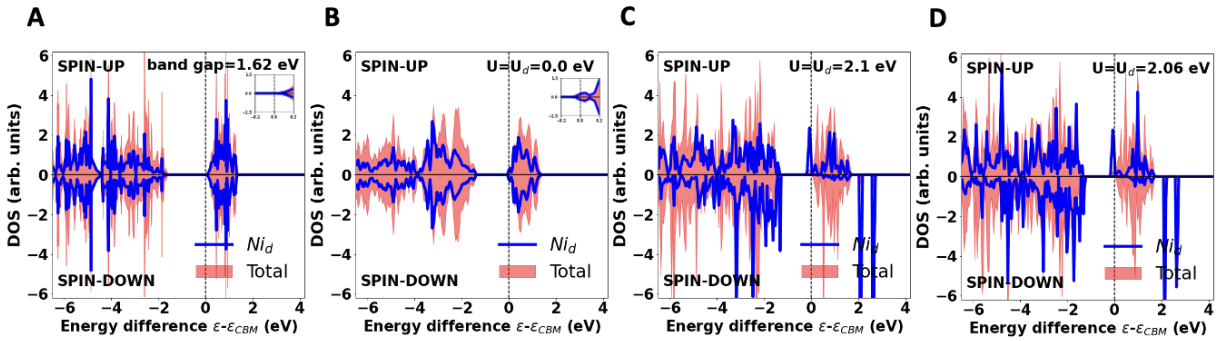

FIG. 5. r^{2}SCAN+rVV10+U+U$_d$ spin-resolved density of states per atom in (A) pristine NiO_2 with Ni(IV) ions with U=U$_d$=2.1 eV and in a single K-intercalated NiO_2 with (B) U=U$_d$ =0.0 eV, (C) U=U$_d$=2.1 eV, (D) U= U$_d$ =2.06 eV. The geometry was optimized in r^{2}SCAN+rVV10+U+U$_d$, which makes the interlayer spacing 5.42 Å. Here we can see one localized occupied state and several localized unoccupied states on the defect Ni(III) cation. The insets in figures A and B show DOS near the 0 eV region. The inset in figure B shows that for U=U$_d$=0 the extra electron from the intercalated K goes to the bottom of the conduction band, making a semi-metal.

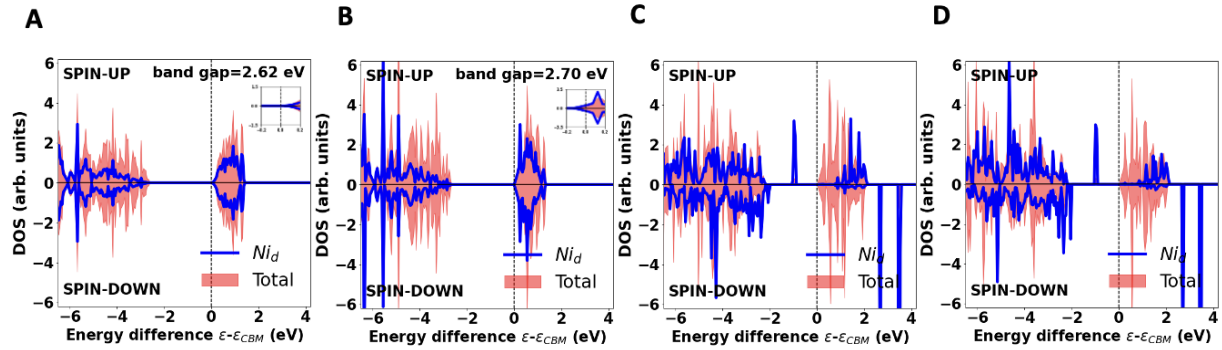

FIG. 6. HSE06+D3 spin-resolved density of states per atom using r^{2}SCAN+rVV10+U+U$_d$ geometry of Fig. 5 in (A) pristine NiO_2 with U=U$_d$=2.1 eV and a single K-intercalated NiO_2 with (B) U=U$_d$=0.0 eV and (C) U=U$_d$=2.1 eV, (D) U= U$_d$=2.06 eV. The insets in figures A and B show DOS near the 0 eV region. The inset in figure B shows that for U=U$_d$=0 the extra electron from the intercalated K goes to the bottom of the conduction band, making a semi-metal.

U=U$_d$=2.06 eV compared to U=U$_d$=2.1 eV. Fig 5D shows r^{2}SCAN+rVV10+U+U$_d$ DOS with U=U$_d$=2.06 eV.

Similar to birnessite, Ni(III) d- states in the VB in Figures 6C and 5D are shifted to higher energy, and there is spin symmetry breaking in total spin DOS in CB, which could be explained with similar reasoning as in birnessite. Here we do not claim U=0.0 eV to be the precise U value for Ni(IV) ions, but we suspect that U could be different than U$_d$ for a K-intercalated NiO_2 system. The accurate determination of U for all the ions in the system would make the r^{2}SCAN+rVV10+U+U$_d$ method more accurate but determining accurate U values is beyond the scope of this work.

The Ni(IV) d-states contain 3 electrons in each spin channel. Due to lower number of electrons in each channel in d-states, it is possible that r^{2}SCAN might induce a different SIE, suggesting a different need of U correc-

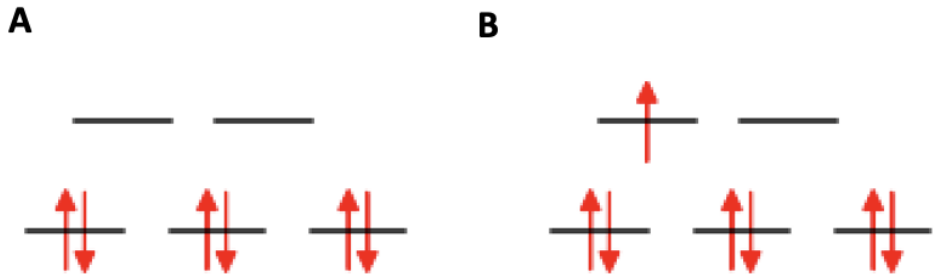

FIG. 7. d-orbital splitting (A) in Ni^{+4} in pristine NiO_2 demonstrating filled t_{2g} states and empty e_g states and (B) in Ni^{+3} in a single K-intercalated NiO_2

tion for Ni(IV) sites. The requirement of a different U for different oxidation states has been observed for Vanadium ions[20]. However, directly observing this phenomenon for the Ni system is challenging, as U determination involves only one oxidation reaction, given the lack of reliable thermodynamic and/or structural data for Ni_2O_3 and NiO_2[20,21]. It is important to note that U=3.0 eV, determined for Co ions (using reaction enthalpies for the oxidation reaction $CoO \rightarrow Co_3O_4$ with an average OS of +2.34 for Co ions), for SCAN+U, can't describe the magnetic and geometric structure of O3-CoO_2 as accurately as SCAN[20]. Additionally, DFT-SCAN correctly predicts metallic behavior in O1-CoO_2, while SCAN+U_{Co} shows a large band gap (1.48 eV)[20,25]. These results suggest that, depending upon the system, description of a defect might require U_d different from U.

We also did HSE06+D3 calculations using r^{2}SCAN+rVV10+U+U_d geometry, and the results are shown in Figure 6. We observe an increase in the band gap of pristine NiO_2, as shown in Fig. 6A. For a single K-intercalated NiO_2, we do not observe polaron formation for U=U_d=0.0 eV, similar to r^{2}SCAN+rVV10+U+U_d as shown in Fig. 6B; however, we observed an increase in the band gap. We also performed HSE06+D3 calculations for U=U_d=2.1 eV and for U=U_d=2.06 eV and obtained DOS as shown in Figures 6C, and 6D, respectively. We observe an increase in the band gap and a shift of the polaron peak deep into the band gap region compared to the corresponding r^{2}SCAN+rVV10+U+U_d DOS. We also observe other effects like shifting of Ni(III) d-states to higher energy and spin symmetry breaking in the total DOS in CB, which could be explained with similar reasoning as above.

We also calculated HSE06 and HSE06+D3 DOS using an exact exchange mixing parameter α of 0.22 on r^{2}SCAN+rVV10+U+U_d geometry with U=U_d=2.1 eV and obtained DOS as shown in Fig. 12 A and B in the supplementary material (SM), respectively. We used the same value of α for Ni, assuming that the α value determined by Peng et al.[1] for Mn won't be very different for Ni as their atomic numbers are not very different. As expected, HSE06(α=0.22) and HSE06(α=0.22)+D3 DOS don't look different. Noticeably, HSE06(α=0.22) DOS doesn't look different from the full HSE06(α=0.25)+D3 evaluated on the same geometry, which is shown in Fig. 6C.

HSE06+D3 essentially repeats the results of r^{2}SCAN+rVV10+U+U_d, with the only difference being the energy shift, and we lack experimental data to validate which method is more correct. However, we can assert that both methods, full r^{2}SCAN+rVV10+U+U_d and HSE06+D3 using the r^{2}SCAN+rVV10+U+U_d geometry with proper U and U_d values, successfully describe defects in a single K-intercalated NiO_2. Among the methods employed to study defect in a K-intercalated NiO_2, full

r^2SCAN+rVV10+U+U_d is notably superfast.

It seems that we may require different U treatment for the defect site than for the non-defect site, as r^2SCAN would exhibit different SIE for these sites. It's also possible that ions in successive oxidation states make very small difference in their SIE. In that case, different U treatments might not be relevant, as U for those oxidation state could be very close or almost equal.

C. Layered $KCoO_2$

We studied another layered material: $KCoO_2$, which has a hexagonal crystal structure with space group $P6_3/mmc$, similar to the above materials MnO_2 and NiO_2. The material project website (https://nextgen.materialsproject.org/) shows a similar material, $LiCoO_2$, with space group $P6_3mc$, to be synthesizable but not stable. The electronic configuration of cobalt d-states is distinct from that of Mn and Ni, as illustrated in Figure 1 in reference[2]. The optimal U value determined for Co ions for r^2SCAN is 1.8 eV[21].

First, we calculated the DOS of $KCoO_2$ using the optimal U value of 1.8 eV and plotted the DOS, as shown in Figure 8A. The band gap of $KCoO_2$ predicted by r^2SCAN+rVV10+U is 2.6 eV. We observed symmetry in the spin resolved total DOS and Co d-states projected onto a Co site. This suggests that Co(III) ions in $KCoO_2$ have zero spin. The zero spin of Co^{+3} is also reported in the work of Chen et al.[26]. The d-state distribution of Co(III) is as shown in Fig. 10A.

The pristine CoO_2 has cobalt d states in a d^5 distribution, and $KCoO_2$ has cobalt in a d^6 distribution. A K-intercalated $KCoO_2$ would have a defect cobalt site in a d^7 distribution, with the remaining Co ions in a d^6 distribution. Co ions in a K-intercalated $KCoO_2$ are in +3 OS, except for the defect site, which is in +2 OS. It is interesting to note that the Co^{+3} ion has no unpaired electron, but Co^{+2} has three unpaired electrons[26]. Chen et al. have proposed d-states of Co^{+2} as shown in figure 7 in their work[26]. So, unlike one electron in e_g the state of defected Ni^{+3} and Mn^{+3}, defected Co^{+2} has four electrons in the e_g states, two in each spin channel[26]. We performed r^2SCAN+rVV10+U+U_d calculations to study the defects in a K- intercalated $KCoO_2$. First, we tried U=U_d=0.0 eV to see how r^2SCAN+rVV10 performs without U correction, and obtained a DOS as shown in figure 8B. The blue plot, which is the PDOS of d-states of the Co^{+2} ion, shows a significant change in the d-state of Co^{+2} compared to the d-state of Co^{+3} ion. Our calculation shows the magnetic moment of the Co^{+2} ion around 3 , indicating three unpaired electrons in d-states. Presence of three unpaired electrons is previously seen in references [37-39]. We observed Co^{+2} d-states splitting as shown in figure 10B. Such splitting is previously reported in ref.[26]. This explains the appearance of Co^{+2} d-states just above the VB maximum in both channels, absence of Co^{+2} d-states in the CB in the up channel and presence in the down channel. Compared to pristine $KCoO_2$, shifting of the Co^{+2} d-states in a single K-intercalated $KCoO_2$ could be attributed to the increased coulomb repulsion in the d-states. There is a breaking of spin symmetry in the DOS, which could be attributed to the dipole formation between K and Co^{+2} ions, which changes the potential of the Co^{+2} containing layer. The phenomena like shifting of d-states to higher energy and spin symmetry breaking in CB are similar to those observed and explained before in Peng et al.'s work[1] in the study of birnessite.

Then we used U=U_d=1.8 eV in r^2SCAN+rVV10+U+U_d and obtained a DOS as shown in figure 8C. The DFA+U method tries to penalize fractional occupation. We don't see much difference between the r^2SCAN+rVV10+U+U_d DOS for U=U_d=0.0 eV and U=U_d=1.8 eV. This indicates that the occupied Kohn-Sham orbitals are well localized and there is no fractional occupancy in r^2SCAN+rVV10+U+U_d calculations with U=U_d=0.0 eV. However, the larger U appears to bring peaks of the

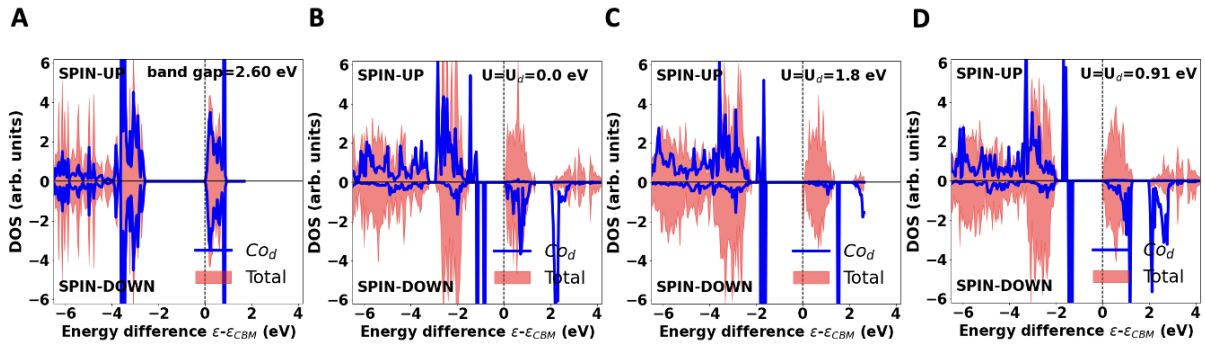

FIG. 8. r^{2}SCAN+rVV10+U spin-resolved density of states per atom in (A) pristine $KCoO_2$ with Co(III) ions with U=U$_d$=1.8 eV, a single K-intercalated $KCoO_2$ with (B) U=U$_d$=0.0 eV, (C) U=U$_d$=1.8 eV, (D) U=U$_d$=0.9 eV. The more complicated pattern of in-gap states could reflect a Co(II) configuration different from a single unpaired electron in an e$_g$ state. Here we see the appearance of several localized occupied states on the defect Co(II) cation. The geometry was optimized in r^{2}SCAN+rVV10+U+U$_d$, which makes the interlayer spacing 5.98 Å. Like the d-states of Ni^{+4}, Co^{+3} has no electron in the e$_g$ state and completely filled t$_{2g}$ states. But, unlike the d-state of Ni^{+3}, which has only one electron in the e$_g$ state and completely filled t$_{2g}$ states, Co^{+2} has four electrons in e$_g$ states, two in each channel, and partially filled t$_{2g}$ states, as shown in figure 10B. The DOS peaks appearing in up and down channels in the gap region of a K-intercalated $KCoO_2$ are due to the e$_g$ electrons in the up and down channels of Co^{+2}, respectively.

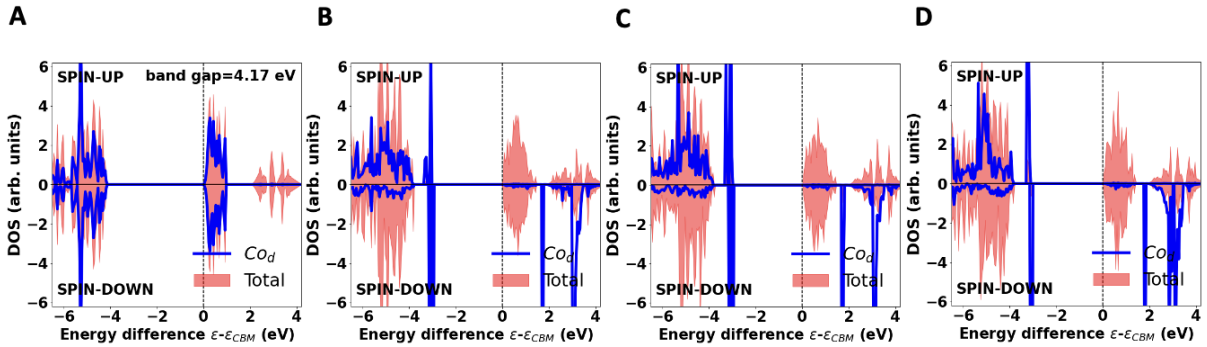

FIG. 9. HSE06+D3 spin-resolved density of states per atom using r^{2}SCAN+rVV10+U+U$_d$ geometry of Fig. 8 in (A) pristine $KCoO_2$ with U=U$_d$=1.8 eV, and in a single K-intercalated $KCoO_2$ with (B) U=U$_d$=0.0 eV, (C) U=U$_d$=1.8 eV, and (D) U=U$_d$=0.9 eV.

defected Co^{+2} d-states closer together in the band gap region just above the VB maximum.

As discussed in the supplementary material, we tried to determine the U value for the Co^{+2} ion by comparing the HSE06+D3 magnetic moment with the r^{2}SCAN+rVV10+U magnetic moment and obtained the U value for the Co^{+2} ion to be 0.91 eV. We couldn't apply the method for Co^{+3} ions as they have zero spin; we used the same U value of 0.91 eV for Co^{+3}. We used U=U$_d$=0.91 eV and obtained a DOS as shown in figure 8D, which looks similar to above result.

We tried to compare a full HSE06+D3 DOS with r^{2}SCAN+rVV10+U+U$_d$ for pristine $KCoO_2$ and a K-intercalated $KCoO_2$. We obtained the $KCoO_2$ supercell by insert-

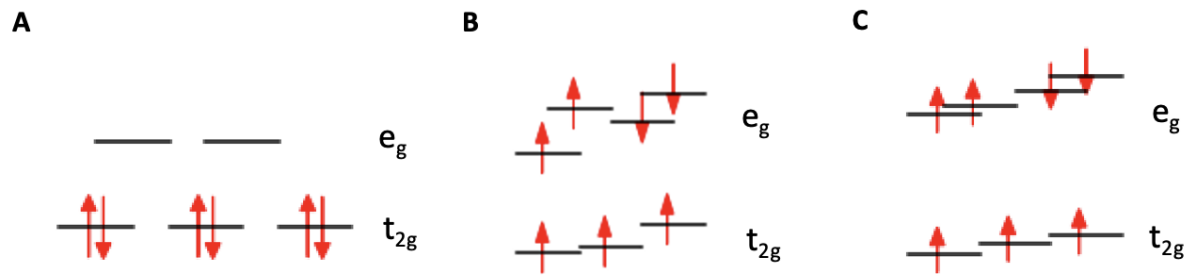

FIG. 10. Schematic diagram of energy of d-orbitals in (A) Co^{+3} in pristine $KCoO_2$ based on HSE06+D3 calculation using r^2SCAN +rVV10+U+U_d geometry with U=U_d=1.8 eV, (B) Co^{+2} in a single K-intercalated $KCoO_2$ based on orbital energy from r^2SCAN+rVV10+U+U_d calculation with U=U_d=1.8 eV and (C) Co^{+2} in a single K-intercalated $KCoO_2$ based on orbital energies from the HSE06+D3 calculation using the r^2SCAN+rVV10+U+U_d geometry with U=U_d=1.8 eV.

ing a K layer for each CoO_2 layer. Compared to the pristine CoO_2 supercell, which contain 96 ions, the $KCoO_2$ supercell has 32 extra K ions, and the K-intercalated $KCoO_2$ supercell has 33 extra K ions. Therefore, one would expect a different lattice parameter for $KCoO_2$ and a K-intercalated $KCoO_2$, which requires the full relaxation of the supercell. We attempted to optimize the structure using the HSE06+D3 method, but it is very challenging for these systems in terms of time and resource. After a month, we chose not to proceed. This is one of the important reasons that motivated us to explore the r^2SCAN+rVV10+U+U_d method, highlighting the significance of the r^2SCAN meta-GGA for defect studies.

However, we calculated the HSE06+D3 DOS using r^2SCAN+rVV10+U+U_d geometry. As shown in figure 9A, HSE06+D3 predicts $KCoO_2$ to be non-magnetic with an increased band gap of 4.17 eV. For a K-intercalated system with r^2SCAN+rVV10+U+U_d geometry, HSE06+D3 DOS is shown in figures 9 B, C, and D for U=U_d=0.0 eV, 1.8 eV, and 0.91 eV, respectively. Here we see that HSE06+D3 not only opens the gap between VB and CB, but it also brings the peaks of the defected Co^{+2} d-states closer together in the band gap region just above the VB maximum. The later effect is similar to r^2SCAN+rVV10+U+U_d result. We observed Co^{+2} d-states splitting as shown in figure 10C for the HSE06+D3 calculation using the r^2SCAN+rVV10+U+U_d geometry with U=U_d=1.8 eV. Such splitting is previously reported in ref.[26]. This explains the appearance of Co^{+2} d-states just above the VB maximum in both the channels, absence of Co^{+2} d-states in CB in the up channel and presence in the down channel. In all HSE06+D3 calculations using r^2SCAN+rVV10+U+U_d geometry, we observed an increase in the band gap, shifting of d-states to higher energy, merging of e_g states in the respective spin channel in the gap region, and spin symmetry breaking of DOS.

Our r^2SCAN+rVV10+U+U_d and HSE06+D3 calculations for a single K-intercalated $KCoO_2$ indicate the defected Co^{+2} ion to have a magnetic moment of around 3 μ_B and we find the same for the Co^{+2} ion in $CaCoO_2$ by the r^2SCAN+rVV10+U(1.8 eV) calculation. The high spin state of Co^{+2} with three unpaired electrons was previously reported in several studies[22,26,27]. These studies also show that an arrangement of O ions around Co^{+2} plays an important role in its d-orbital splitting. In the case of a symmetrical tetrahedral CoO_6 arrangement, the d-orbitals of Co ions split into t_{2g} and e_g states, as shown in Fig 10A. There are several factors that can lead to different

arrangements of d-orbitals in Co ions. In a recent work by Kim et al.[27] on $CaCoO_2$, a Co^{+2} ion bonds with four oxygen ions in a plane and shows three types of Co^{+2} ions with different PDOS of d states, as shown in figures 4d and extended data 5d and e, indicating different d-orbital arrangements. In the same work, figs. 1 and 4d clearly show that Co^{+2} d-orbital splitting depends on the Co^{+2} environment. In the other work by Chen et al.[26] on cobalt oxide Co_3O_4, which contains cobalt ions in two different oxidation states Co^{+2} and Co^{+3}, which are located at interstitial tetrahedral and octahedral sites, respectively, it has also been reported that there are three unpaired electrons in Co^{+2} with d-orbital splitting as shown in Fig. 7. In a different work by Bunting et al.[22] on a molecule $Co(C(SiMe_2ONaph)_3)_2$, the high spin electronic configuration of the Co^{+2} ion was reported. A common finding of these studies is that Co^{+2} has three unpaired electrons, and its d-orbital arrangement is not unique but rather very sensitive to the arrangement of ions around it.

Fig. 13 in SM shows Co^{+2}-O bond lengths in angstrom units and Fig. 14 in SM shows PDOS of Co^{+2} d-states in a single K-intercalated $KCoO_2$. We see that all the d-states in the spin-up channel in Fig. 14 in SM are occupied, indicating five electrons in the spin-up channel. To get a rough estimate of the number of d-electrons in the Co^{+2} ion in a different region of the DOS plot in a single K-intercalated $KCoO_2$, we integrated the PDOS shown in Fig. 9C and found 2.3 electrons in VB and 3.6 in CB in the spin-down channel and 6.7 in VB and 0.0 in the CB in spin up channel. Please note that these could not be the exact number of electrons as PDOS is due to the charge density in the Weigner-Seitz sphere, which does not measure the charge of the ion in the solids. However, these rough estimates indicate that there are a total of two electrons in the d-orbitals in the spin-down channel and five electrons in the spin-up channel, supporting the d_7 configuration of Co^{+2} with three unpaired electrons. The "EIGENVAL" file in VASP calculation also shows three extra electrons in spin-up channel compared to spin-down channel.

To get more details on the d-states of the Co^{+2}, we also obtained the r^2SCAN+rVV10+U with U=1.8 eV total DOS and PDOS of a pristine $CaCoO_2$, as shown in Fig. 15 in SM A. We also plotted individual PDOS of Co^{+2} d-orbitals as shown in Fig. 17 in SM. The $CaCoO_2$ bilayer supercell with 128 atoms was used in our calculation, where Ca ions were sandwiched between CoO_2 layers such that Ca:Co=1:1. The structure is fully relaxed using the r^2SCAN+rVV10+U(1.8 eV) functional. Our calculation shows two types of Co^{+2}-O bond lengths of 2.178Å and 2.182Å in pristine $CaCoO_2$, as shown in Fig. 16 in SM. However, the r^2SCAN+rVV10+U calculation with U = 1.8 eV using a bilayer $CaCoO_2$ small cell with eight ions shows no distortion in the CoO6 tetrahedron and metallic nature, as shown in Fig. 15 B in SM. The bigger cell opens a band gap due to small distortions in the CoO6 tetrahedron. Compared to the $KCoO_2$ DOS, as shown in figures 8A and 9A, there is an appearance of DOS in the band gap region of pristine $CaCoO_2$ in both spin channels. We also estimated the rough number of electrons by integrating PDOS and found 2.6 electrons in VB and 3.2 in CB in the spin-down channel and 5.6 in VB and 0.0 in CB in the spin-up channel. This supports the d_7 distribution of Co^{+2} with three unpaired electrons in the spin-up channel in pristine bilayer $CaCoO_2$. As shown in Fig. 15 A in SM, we also integrated PDOS in the "gap region" and found 0.7 electrons in the spin-up channel and 1.9 electrons in the spin down channel. This suggests that electrons in the down channel are more localized in the gap region. As shown Fig. 15 A in SM, the PDOS in the gap region in the up channel is mainly due to dyz, dxz, and dx^2-y^2 orbitals that are delocalized deep in the VB. This explains why integrating the gap region in the up channel gives only 0.7 electrons. Figures 13 and 16 in SM clearly differ from each other, which explains the reason for the

difference in d-states of Co^{+2} ions in a single K-intercalated $KCoO_2$ and pristine $CaCoO_2$.

We plotted the HSE06+D3 energy of Co^{+2} occupied d-orbitals evaluated at the gamma point in a single K-intercalated $KCoO_2$ using r^{2}SCAN+rVV10+U+U_d geometry with U=U_d=1.8 eV as shown in figure 10C. We observe splitting in e_g spin-up and spin-down orbitals. The higher energy of spin-down dz^2 and dx^2-y^2 could be due to increased coulomb repulsion between these orbitals and sp^3 hybridized orbitals of oxygen. This also explains why the distorted tetrahedron as shown in Fig. 13 in SM, has two of the bonds between defected Co^{+2} and O nearly 15% longer compared other remaining four bonds. The spin due to e_g orbitals in the majority channel could be cancelling the spin due to e_g orbitals in the minority channel giving a high spin state of Co^{+2} ion with three unpaired electrons in a single K-intercalated $KCoO_2$. This arrangement of d-orbitals is similar to Fig. 7 in the work by Chen et al.[26].

We can say that the r^{2}SCAN+rVV10+U+U_d method successfully described the point defect in a K-intercalated $KCoO_2$ and was much faster compared to expensive hybrid functions like HSE06. The use of r^{2}SCAN+rVV10+U+U_d geometry and wavefunction to conduct further HSE06+D3 calculations for obtaining the electronic structure of defects in solids could be a way to describe defects which is as accurate as full HSE06+D3 method, but much faster.

III. CONCLUSIONS

Defects in solids can be utilized to tune the electronic structure of materials, impacting applications in various fields. Defects can be investigated using first-principles calculations with DFT. However, DFAs introduce SIE that could vary depending on the element, system, site, and oxidation state, hindering the performance of DFAs. Hybrid functionals mitigate SIE by mixing exact exchange , but at the expense of computational cost, successfully describing defects in many materials. The computational cost of hybrid functionals increases significantly for a SCF (self-consistent field) calculation compared to meta-GGAs like r^{2}SCAN. Defect studies require large supercells, making SCF calculations very expensive. Ionic relaxation calculations for defect studies involve many SCF cycles, making the process cumbersome for a hybrid functional to optimize the structure.

Here we demonstrate that the r^{2}SCAN+rVV10+U+U_d method can successfully describe defects in materials with proper values of U and U_d. The method is much faster than hybrid functionals but equally accurate. Using r^{2}SCAN+rVV10+U+U_d geometry enables the completion of hybrid functional calculations in a reasonable time and with fewer resources. This approach makes hybrid functional calculations feasible for larger systems with transition-metal ions.

The r^{2}SCAN+rVV10+U+U_d method proposed here is not only faster but as accurate as the already established hybrid functional method for defect studies. This method will expedite the study of defects in materials and contribute to the rapid growth of the field. The r^{2}SCAN+rVV10+U+U_d method can also be employed in systems without defects where ions of the same species are in different OS.

We have studied the layered oxides MnO_2, NiO_2, and $KCoO_2$, both in the pristine state and with one K atom intercalated between layers in a supercell. Inexpensive r^{2}SCAN+rVV10+U+U_d equilibrium geometries have been used for electronic structure calculations with r^{2}SCAN+rVV10+U+U_d and with the expensive HSE06 hybrid functional. For K-intercalated MnO_2 and NiO_2, we find no localized e_g state on the defected transition metal ion for U-U_d=0, but we find one such state for standard positive U values. This state, in the gap between conduction and valence bands accepts the electron donated by the intercalated K. (For U=U_d=0, the extra electron from the intercalated K goes into the bottom of the conduction band, making the intercalated material

a semi-metal. The extra electron is then delocalized over the supercell, with fractional occupation on each transition-metal ion.)

For K-intercalated $KCoO_2$, both for $U=U_d=0$ (standard semilocal r^{2}SCAN without a nonlocal +U self-interaction correction) and for standard positive U values, we seem to find two majority-spin and two minority-spin occupied localized e_g states in the gap between valence and conduction bands, and three empty localized minority-spin t_{2g} states in the gap above the conduction band. This surprising result is consistent with a dramatic change in the electronic configuration (Fig. 10) from the undefected Co^{+3} ions to the defected Co^{+2} ion, as reported previously in Ref.[26].

IV. COMPUTATIONAL DETAILS

First-principles calculations were performed with the projector-augmented wave method[28], implemented in the VASP code[29,30]. A 4 x 4 x 2 supercell was used to simulate defects in layered TMOs. For all supercell calculations, a 2 x 2 x 2 Γ-centered Monkhorst-Pack k mesh[31] was used.

For r^{2}SCAN+rVV10+U+U_d calculations, a 500 eV cutoff for the plane waves was used. In all r^{2}SCAN+rVV10+U+U_d calculations, the cell volume was relaxed with the ISIF=3 setting until forces converged to less than 0.03 eV/Å and energy converged to less than 10^{-6} eV. To conduct r^{2}SCAN+rVV10+U+U_d calculations, we employed the simplified rotationally invariant framework developed by Dudarev et al.[32].

For HSE (as for r^{2}SCAN+rVV10+U+U_d), corrections due to the periodic boundary condition and the supercell size have been added[1,33]. For figure 1, we used an exact mixing parameter α of 0.22 in the hybrid functional HSE06[1,34], as determined from the Generalized Koopman's Condition (GKC) method[35–38]. For all the remaining HSE06+D3 calculations, we used the standard exact exchange mixing parameter of 0.25. A plane-wave basis with an energy cutoff of 400 eV was employed.

V. ACKNOWLEDGMENTS

This work was supported by the U.S. Department of Energy, Office of Science Basic Energy Sciences under Award No. DE-SC0023356.

[1] H. Peng, I. G. McKendry, R. Ding, A. C. Thenuwara, Q. Kang, S. L. Shumlas, D. R. Strongin, M. J. Zdilla, and J. P. Perdew, PNAS **114**, 9523 (2017).

[2] R. Ding, P. Yasini, H. P. Peng, J. P. Perdew, E. Borguet, and M. J. Zdilla, Adv. Energy Mater. **11**, 2101636 (2021).

[3] P. Hohenberg and W. Kohn, Phys. Rev. **136**, B864 (1964)).

[4] W. Kohn and L. J. Sham, Phys. Rev. **140**, A1133 (1965).

[5] J. P. Perdew, R. G. Parr, M. Levy, and J. L. Balduz, Jr., Phys. Rev. Lett. **49**, 1691 (1982).

[6] J. Sun, R. C. Remsing, Y. Zhang, Z. Sun, A. Ruzsinszky, H. Peng, Z. Yang, A. Paul, U. Waghmare, X. Wu, M. L. Klein, and J. P. Perdew, Nature Chemistry **08**, 831 (2016).

[7] T. M. Henderson, J. Paier, , and G. E. Scuseria, Phys. Status Solidi B **248**, 767 (2011).

[8] J. W. Furness, A. D. Kaplan, J. Ning, J. P. Perdew, and J. Sun, J. Phys. Chem. Lett. **11**, 8208 (2020).

[9] A. P. Bartók and J. R. Yates, J. Chem. Phys. **150**, 161101 (2019).

[10] J. W. Furness, A. D. Kaplan, J. Ning, and J. P. Perdew, J. Phys. Chem. Lett. **11**, 8208 (2020).

[11] H.-D. Saÿnick and C. Cocchi, Electron. Struct. **3**, 027001 (2021).

[12] D. Wickramaratne and J. L. Lyons, ArXiv:2311.03634v1.

[13] A. Varadwaj and T. Miyake, Electron. Struct. **7**, e20220017 (2022).
[14] V. I. Anisimov, J. Zaanen, , and O. K. Andersen, Phys. Rev. B **44**, 943 (1991).
[15] V. I. Anisimov, I. V. Solovyev, M. A. Korotin, M. T. Czyzyk, , and G. A. Sawatzky, Phys. Rev. B **48**, 16929 (1993).
[16] I. V. Solovyev, P. H. Dederichs, , and V. I. Anisimov, Phys. Rev. B **50**, 16861 (1994).
[17] M. Cococcioni and S. de Gironcoli, Phys. Rev. B **71**, 035105 (2005).
[18] O. A. Vydrov and T. V. Voorhis, J. Chem. Phys. **133**, 244103 (2010).
[19] R. Sabatini, T. Gorni, and S. de Gironcoli, Physical Review Material **4**, 045401 (2020).
[20] O. Y. Long, G. S. Gautam, and E. A. Carter, Physical Review Material **4**, 045401 (2020).
[21] S. Swathilakshmi, R. Devi, and G. S. Gautam, J. Chem. Theory Comput. **19**, 4202 (2023).
[22] P. C. Bunting, M. Atanasov, E. Damgaard-Møller, M. Perfetti, I. Crassee, M. Orlita, J. Overgaard, J. V. Slageren, F. Neese, and J. R. Long, Science **362**, 1378 (2018).
[23] J. Jonas and S. Grimme, J. Phys. Chem. C **118**, 7615 (2014).
[24] J. M. P. Martirez and E. A. Carter, J. Am. Chem. Soc. **141**, 693 (2019).
[25] T. Motohashi, T. Ono, Y. Sugimoto, Y. Masubuchi, S. Kikkawa, R. Kanno, M. Karppinen, and H. Yamauchi, Phys. Rev. B **80**, 165114 (2009).
[26] J. Chen, X. Wu, and A. Selloni, Phy. Rev. B **83**, 245204 (2011).
[27] W. J. Kim, M. A. Smeaton, C. Jia, B. H. Goodge, B. G. Cho, K. Lee, M. Osada, D. Jost, A. V. Ievlev, B. Moritz, L. F. Kourkoutis, T. P. Devereaux, and H. Y. Hwang, Nature **615**, 237 (2023).
[28] P. E. Blöchl, Phys. Rev. B **50**, 17953 (1994).
[29] G. Kresse and J. Hafner, Phys. Rev. B Condens Matter **49**, 14251–14269 (1994).
[30] G. K. G and D. Joubert, Phys. Rev. B **59**, 1758–1775 (1999).
[31] H. Monkhorst and J. Pack, Phys. Rev. B **13**, 5188–5192 (1976).
[32] S. L. Dudarev, G. A. Botton, S. Y. Savrasov, C. J. Humphreys, and A. P. Sutton, Phys. Rev. B **57**, 1505 (1998).
[33] Y. Kumagai and F. Oba, Phys. Rev. B **89**, 195205 (2014).
[34] A. Krukau, O. Vydrov, A. Izmaylov, and G. Scuseria, J. Chem. Phys. **125**, 224106 (2006).
[35] S. Lany and A. Zunger, Phys. Rev. B **80**, 085202 (2009).
[36] S. Lany, Phys. Status Solidi B **248**, 1052–1060 (2011).
[37] H. Peng and S. Lany, Phys. Rev. B **85**, 201202 (2012).
[38] H. Peng, P. Ndione, D. Ginley, A. Zakutayev, and S. Lany, Phys. Rev. X **5**, 021016 (2015).

Supplementary Material

Determination of Hubbard U correction

To determine the Hubbard U correction, we compared the HSE06+D3 magnetic moment (MM) of ions inside the Weigner-Seitz sphere with the r^{2}SCAN+rVV10+U's MM. First, we relaxed the structure using the HSE06+D3 method and used this structure to calculate the HSE06+D3 MM. We then used the HSE06+D3 structure to do the r^{2}SCAN+rVV10+U calculation, where we slowly varied the U value until r^{2}SCAN+rVV10+U's MM becomes equal to the HSE06+D3's MM. We used smaller bilayer unit cells of transition metal oxides for U determination using this method. We used MnO_2, $KMnO_2$, $KNiO_2$, and $CaCoO_2$ to get U values for Mn^{+4}, Mn^{+3}, Ni^{+3}, and Co^{+2} ions, respectively. All calculations are performed using VASP code, where we used Γ-centered Monkhorst-pack grid of size 8 x 8 x 8 and a cut off energy of 400 eV for plane wave basis.

First, we used HSE06+D3 with an exact exchange mixing parameter (α) of 0.22 to be consistent with Peng et. al.'s work[1]. We have summarized the calculated U value for these ions in Table I below.

	HSE06($\alpha = 0.22$)+D3 MN (μ_B)	r^{2}SCAN+rVV10+U MM (μ_B)	U (eV)
MnO_2	3.023	3.023	1.41
$KMnO_2$	3.933	3.933	1.26
$KNiO_2$	1.098	1.098	1.53
$CaCoO_2$	2.663	2.663	0.55

TABLE I. The U value determination by comparing the magnetic moment (MM) of HSE06+D3 with r^{2}SCAN+rVV10+U using HSE06+D3 geometry for both functionals.

We couldn't use this method to determine the U values for Ni^{+4} and Co^{+3} ions using NiO_2 and $KCoO_2$ systems because the MM of Ni^{+4} and Co^{+3} ions in NiO_2 and $KCoO_2$ being zero, and these MMs are zero and largely independent of U values in the r^{2}SCAN+rVV10+U calculation. So, we used the same U values for Ni^{+4} and Co^{+3} as determined for Ni^{+3} and Co^{+4}, respectively. We used the U values determined in Table I, as well as U values from the literature[2], and calculated lattice parameters for MnO_2, NiO_2, and $CaCoO_2$ unit cells to see how r^{2}SCAN+rVV10+U performs compared to HSE06+D3 with α=0.22. The results are summarized in the Table II below. We see that the lattice constants agree well for r^{2}SCAN+rVV10 and r^{2}SCAN+rVV10+U, but they disagree with HSE06+D3 (α=0.22) lattice parameters, especially the c parameter. This motivated us to go back to full HSE06.

As above, we again determined U values by comparing the MM of r^{2}SCAN+rVV10+U with the full HSE06+D3 (α=0.25) functional. Table III below summarizes the result. The U values determined in the Table III are closer to the values in the literature, where optimal values for Mn, Ni, and Co ions for r^{2}SCAN are 1.8 eV, 2.1 eV, and 1.8 eV, respectively[2]. The difference in oxidation states of ions could be the cause of the discrepancy. We used the above U values for the r^{2}SCAN+rVV10+U functional and again compared the lattice parameters. The results are summarized in Table IV below.

System	Method	Lattice Parameters (Å)			Lattice Angles (Degree)		
		a	b	c	α	β	γ
MnO_2	r^2SCAN+rVV10	2.82	2.82	9.23	90	90	120
	r^2SCAN+rVV10+U(1.41 eV)	2.83	2.83	9.22	90	90	120
	HSE06($\alpha = 0.22$)+D3	2.83	2.83	9.59	90	90	120
NiO_2	r^2SCAN+rVV10	2.74	2.74	8.98	90	90	120
	r^2SCAN+rVV10+U(1.53 eV)	2.73	2.73	9.00	90	90	120
	HSE06($\alpha = 0.22$)+D3	2.72	2.72	9.25	90	90	120
$KCoO_2$	r^2SCAN+rVV10	2.89	2.89	11.64	90	90	120
	r^2SCAN+rVV10+U(0.55 eV)	2.89	2.89	11.65	90	90	120
	HSE06($\alpha = 0.22$)+D3	2.86	2.86	11.21	90	90	120

TABLE II. Lattice parameters and lattice angles comparison for r^2SCAN+rVV10, r^2SCAN+rVV10+U and HSE06($\alpha = 0.22$)+D3 methods for the systems MnO_2, NiO_2 and $KCoO_2$.

	HSE06($\alpha = 0.25$)+D3 MN (μ_B)	r^2SCAN+rVV10+U MM (μ_B)	U (eV)
MnO_2	3.036	3.036	1.71
$KMnO_2$	3.947	3.947	1.58
$KNiO_2$	1.163	1.163	2.06
$CaCoO_2$	2.683	2.683	0.91

TABLE III. The U value determination by comparing the magnetic moment (MM) of HSE06+D3 with r^2SCAN+rVV10+U using HSE06+D3 geometry for both functionals.

System	Method	Lattice Parameters (Å)			Lattice Angles (Degree)		
		a	b	c	α	β	γ
MnO_2	r^2SCAN+rVV10	2.82	2.82	9.23	90	90	120
	r^2SCAN+rVV10+U(1.71 eV)	2.84	2.84	9.11	90	90	120
	HSE06($\alpha = 0.25$)+D3	2.82	2.82	9.25	90	90	120
NiO_2	r^2SCAN+rVV10	2.74	2.74	8.98	90	90	120
	r^2SCAN+rVV10+U(2.06 eV)	2.73	2.73	8.98	90	90	120
	HSE06($\alpha = 0.25$)+D3	2.73	2.73	9.03	90	90	120
$KCoO_2$	r^2SCAN+rVV10	2.89	2.89	11.64	90	90	120
	r^2SCAN+rVV10+U(0.91 eV)	2.89	2.89	11.65	90	90	120
	HSE06($\alpha = 0.25$)+D3	2.87	2.87	11.61	90	90	120

TABLE IV. Lattice parameters and lattice angles comparison for r^2SCAN+rVV10, r^2SCAN+rVV10+U and HSE06($\alpha = 0.25$)+D3 methods for the systems MnO_2, NiO_2 and $KCoO_2$.

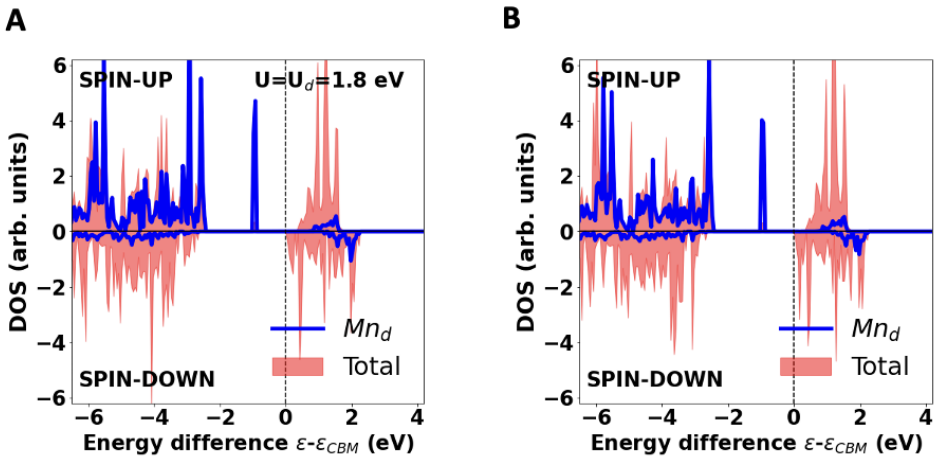

FIG. 11. Spin-resolved density of states per atom using r^{2}SCAN+rVV10+U+U$_d$ (with U=U$_d$=1.8 eV) geometry in a single K-intercalated MnO_2 using (A) HSE06 (with α=0.22) and (B) HSE06 (with α=0.22)+D3.

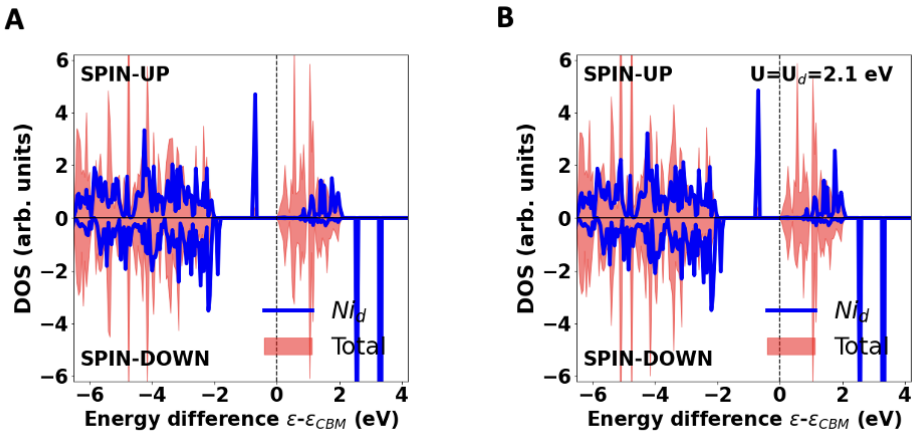

FIG. 12. Spin-resolved density of states per atom using r^{2}SCAN+rVV10+U+U$_d$ (with U=U$_d$=2.1 eV) geometry in a single K-intercalated NiO_2 using (A) HSE06 (α=0.22) and (B) HSE06 (α=0.22)+D3.

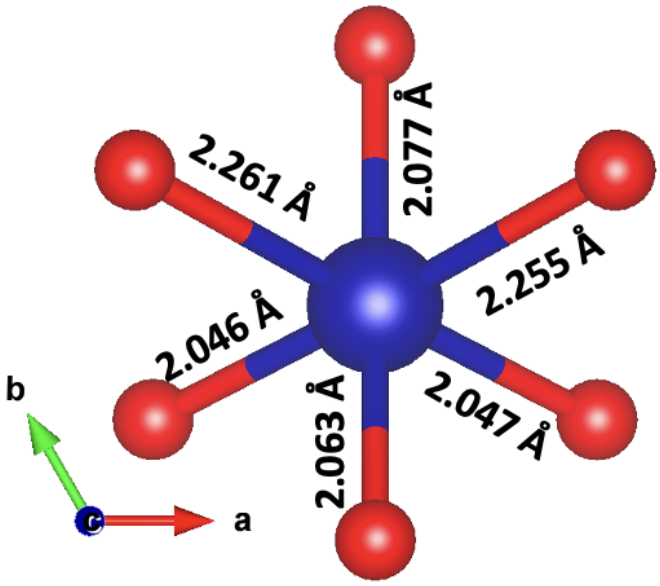

FIG. 13. Co^{+2} - O bond lengths in a K-intercalated $KCoO_2$ show the symmetry breaking of the CoO6 tetrahedron. All lengths are in angstrom units. The red balls represent O ions and blue Co^{+2} ions.

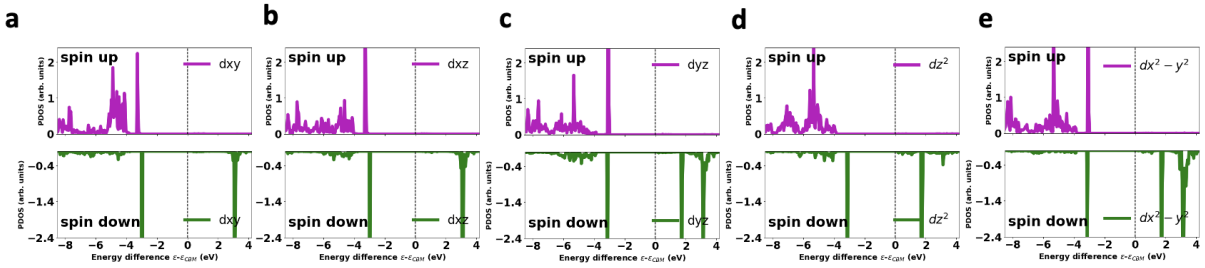

FIG. 14. HSE06(α=0.25)+D3 spin resolved PDOS of Co^{+2} d-states in a single K-intercalated $KCoO_2$. To obtain HSE06+D3 DOS, we used r^2SCAN+rVV10+U+U_d (U=U_d=1.8 eV) geometry. The absence of PDOS in the CB in the up channel indicates complete occupancy of all up channel d-states. The remaining two electrons of Co^{+2} d^7 state are in the down channel and delocalized.

Integrated PDOS range	Estimated Number of Electrons	
	Spin Up	Spin Down
VB	5.6	2.6
CB	0.0	3.2
Gap region (shown in Fig. 15 A)	0.7	1.9

TABLE V. Estimated number of electrons in different regions of PDOS of Co^{+2} d-orbitals obtained by integrating PDOS in pristine $CaCoO_2$ from r^2SCAN+rVV10+U+U_d (U=U_d=1.8 eV). Fig. 14 shows that PDOS in the gap region in the spin-up channel is mainly due to dyz, dxz, and dx^2-y^2 orbitals, which have dispersed deep into the VB. So, integrating only the gap region, as shown in Fig. 13, didn't give a number close to two.

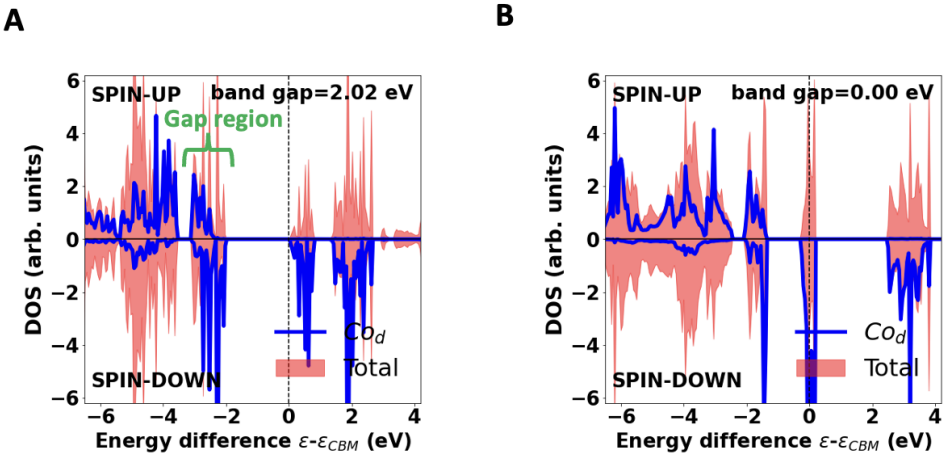

FIG. 15. Pristine $CaCoO_2$ spin-resolved density of states per atom using r^2SCAN+rVV10+U+U_d (U=U_d=1.8 eV) using (A) a supercell with 128 ions and (B) a small cell with eight ions. Calculation using the smaller cell shows a metallic solution, and the larger cell opens a band gap.

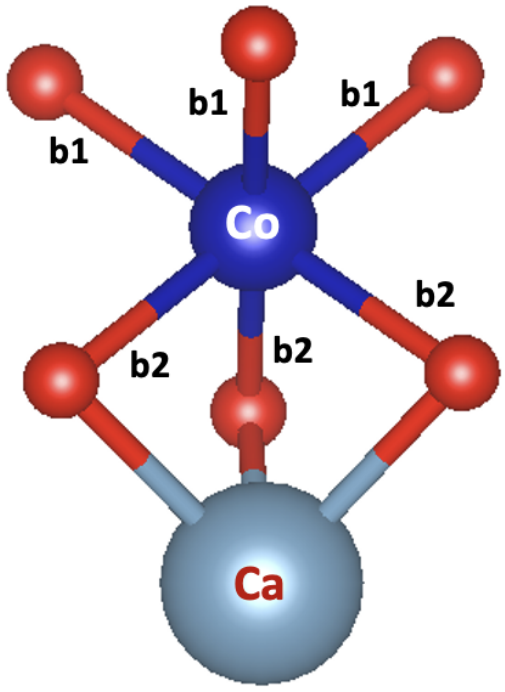

FIG. 16. Co^{+2} - O bond lengths in a pristine $CaCoO_2$ supercell show the symmetry breaking of the CoO6 tetrahedron. The values of b1 and b2 are 2.178Å and 2.182Å, respectively, and all lengths are in angstrom units. The red, blue, and cyan balls represent O, Co, and Ca ions, respectively.

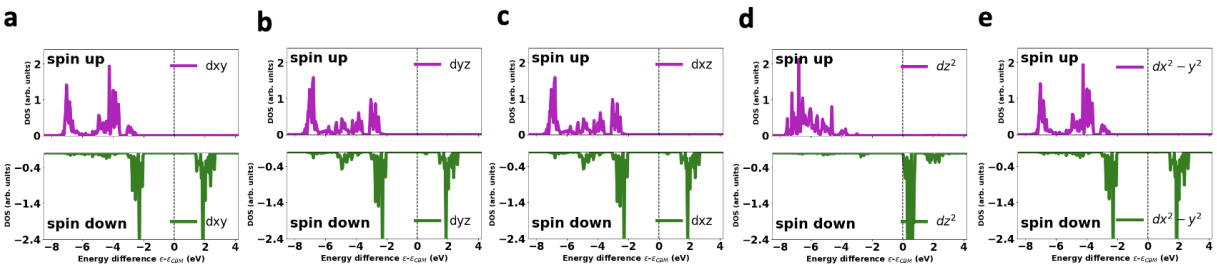

FIG. 17. The spin-resolved PDOS of Co^{+2} d-orbitals in $CaCoO_2$ supercell from r^2SCAN+rVV10+U+U_d (U=U_d=1.8 eV).